

Static surface mode expansion for the full-wave scattering from penetrable objects

Carlo Forestiere, Giovanni Gravina, Giovanni Miano, Guglielmo Rubinacci, Antonello Tamburrino

Abstract—We introduce longitudinal and transverse static surface modes and use them to solve the surface integral equation governing the full-wave electromagnetic scattering from penetrable objects. The longitudinal modes are the eigenmodes with zero surface curl of the electrostatic surface integral operator, which gives the scalar potential as a function of the surface charge density. The transverse modes are the eigenmodes with zero surface divergence of the magnetostatic surface integral operator, which returns the vector potential as a function of the surface current distribution. These modes are orthogonal. The static modes only depends on the shape of the object, thus, the same static basis can be used regardless of the frequency of operation and of the material constituting the object. We expand the unknown surface currents of the Poggio-Miller-Chang-Harrington-Wu-Tsai surface integral equations in terms of the static surface modes and solve them using the Galerkin-projection scheme. The introduced expansion allows the regularization of the singular integral operators and yields a drastic reduction of the number of unknowns compared to a discretization based on standard sub-domain basis functions.

I. INTRODUCTION

The analysis and design of electromagnetic scattering from a collection of mutually coupled dielectric objects is of great importance for many applications, spanning from antennas arrays [1] to metasurfaces [2] and metalens [3]. In this context, the use of integral formulations is appealing since the unknowns are defined only within the object's volume or - if the object is spatially piecewise homogeneous - on its boundary and internal interfaces, while the radiation conditions at infinity are naturally satisfied. Nevertheless, the corresponding discrete problem is characterized by dense matrices, and their inversion is usually associated with high computational burden, even when acceleration techniques [4] like fast multipole algorithms are implemented.

Accurate and efficient solutions of integral formulations heavily depend on the choice of basis functions. Two macro-categories of basis functions may be identified: *sub-domain* functions, which are non-zero only over a portion of the object, or *entire-domain* functions, which extend over the entire domain of one or few individual objects. Although the former approach may have a wider applicability, and is arguably more robust when dealing with objects of irregular shape and sharp

corners, the latter is very appealing when multiple scattering problems are considered, where the electromagnetic system under investigation is a collection of mutually-coupled objects [5], [6], [7].

Representative examples of sub-domain functions are those involved in the finite element method and discontinuous Galerkin method [8]: for instance the Rao-Wilton-Glisson rooftop functions [9], loop-star functions [10], [11], [12], [13], loop-tree functions [14], Trintinalia-Ling functions [15], Buffa-Christiansen functions [16], higher order vector basis functions of the Nedelec type [17], etc..

Dually, classic examples of entire-domain basis functions are the vector spherical wave functions (see for instance [18]), vector spheroidal wave functions [19]. Analytic entire domain basis functions may be generated in coordinate systems where the Helmholtz equation is separable. A different but effective strategy to generate entire domain basis functions even in irregular domains is by introducing a convenient auxiliary eigenvalue problem. This is done for instance with characteristic modes [20], [21], [22], [23], (see [5], [6] for arrays of perfectly conductive particles and [24] for metal metasurfaces). The characteristic modes do not depend on the particular excitation conditions, and they are effective in the numerical solution of the problems of electromagnetic scattering from collections of objects of given material at a fixed operating frequency. Nevertheless, characteristic modes do depend on the frequency, and their interesting properties are lost if they are used as a basis at a frequency different from the one at which they are computed. Thus, they may not be the best choice when multiple frequencies are involved since they have to be recalculated at each frequency.

In this paper, we look for a different set of entire domain basis functions, that can simplify the numerical solution of electromagnetic scattering problems from a given object at multiple frequencies. We investigate the use of static surface current modes as an entire-domain basis set to represent the unknown current densities in surface integral equation formulations. These modes are the union of two sets: longitudinal and transverse modes, exhibiting vanishing surface curl and surface divergence, respectively. We assemble these two sets by solving two auxiliary frequency-independent eigenvalue problems, involving Hermitian and positive-definite surface-integral operators, having the *static* Green function as kernel. We demonstrate that the use of these modes in the Galerkin projection of the Poggio-Miller-Chang-Harrington-Wu-Tsai surface integral formulation [25] leads to a drastic reduction of the number of unknowns with respect to sub-domain basis functions without deteriorating the accuracy of

C. Forestiere, G. Gravina G. Miano, G. Rubinacci are with the Department of Electrical Engineering and Information Technology, Università degli Studi di Napoli Federico II, via Claudio 21, Napoli, 80125, Italy

G. Gravina is with 10th Aircraft Maintenance Department, Italian Air Force, Viale dell'Aeronautica 1, 73013 Galatina, Lecce, Italy

A. Tamburrino is with Dipartimento di Ingegneria Elettrica e dell'Informazione "M. Scarano", Università degli Studi di Cassino e del Lazio Meridionale, Via G. Di Biasio n. 43, 03043 Cassino (FR), Italy

the solution. The static modes are the low-frequency limit of resonance modes of surfaces of finite conductivity [26]. Their volume counterparts have been presented in Ref. [27], [28] (longitudinal) and in Ref. [29] (transverse) where they have been already used to expand the electromagnetic field [30], [31], [32].

The proposed approach shares similarities with the one introduced by Vecchi et al. and used in a hybrid spectral-spatial method for the analysis of printed antennas [33], [34].

There are several attributes that make the static surface modes particularly interesting

- For objects of size comparable to the wavelength of operation only few modes are sufficient to describe the emergent scattering response. This property also holds true when multiple scattering problems are considered, namely when the electromagnetic system is a collection of mutually-coupled objects as long as the objects are not too close to each other. These characteristics are particularly appealing for the numerical modeling of metasurfaces and metalens.
- The retarded Green function, constituting the kernel of integral operators recurring in surface integral formulations such as the PMCHWT, may be decomposed as the sum of the static Green function (with integrable singularity) and a proper difference (which is a regular function); the resulting integral operators containing the static Green function are diagonalized by the static modes, thus the overall problem is regularized [35].
- The use of the static modes expansion combined with an appropriate rescaling and rearranging of the unknowns makes the PMCHWT formulation immune from the low-frequency breakdown problem, which otherwise plagues it due to the different frequency scaling of the involved operators.
- The static modes only depend on the shape of the object, thus, the same static basis can be used (and has the same advantages) regardless of the operating frequency and material of object. This fact enables the description of any scattering scenario involving one or more objects of a given shape, in terms of the same “alphabet” of basis function, regardless of the frequency of operation. This fact constitutes a great advantage compared to other basis sets (e.g., characteristic modes), where the modes depend on frequency and materials, thus the alphabet of basis functions, in which the scattering process is described, changes every time one of these parameters is varied, thus preventing a unified description.

The paper is organized as follows: in Sec. II we introduce the static basis and its numerical generation, then in Sec. III we recall the Poggio-Miller-Chang-Harrington-Wu-Tsai formulation and we show that the static mode expansion regularizes the involved operator, and a proper rescaling of the unknowns makes this formulation immune from the low-frequency breakdown. In Sec. IV we perform several numerical experiments. We validate the introduced method in two resonant scattering problems, namely the scattering from a metal particle and high-permittivity particle in the visible/near-infrared spectral

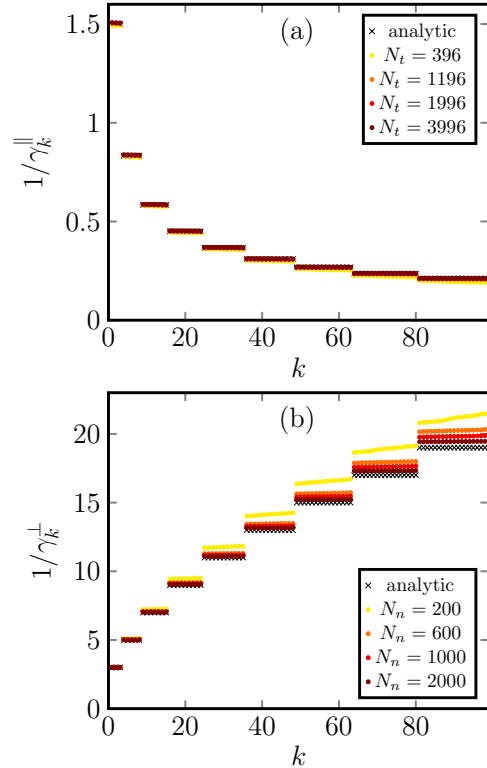


Fig. 1. Reciprocal of the first 100 eigenvalues γ_k^{\parallel} (a) and γ_k^{\perp} (b) associated with the longitudinal and transverse static modes of a sphere, respectively, and computed for several densities of the triangular surface mesh (filled circles of different colors) having N_t elements and N_n nodes. The eigenvalues are compared with their analytical value.

range. We consider a sphere, where there exists an analytical solution, and a rod, which is a shape often recurring in the context of nano-optics. In all investigated cases, for particles of dimensions comparable to the incident wavelength, we demonstrate that only a few modes are required to describe the electromagnetic scattering response. Eventually in Sec. VI we draw the conclusions.

II. STATIC SURFACE CURRENT MODES

We denote with Ω a bounded three-dimensional domain, with $\partial\Omega$ its boundary, with $\hat{\mathbf{n}}$ the normal to the surface $\partial\Omega$ pointing outward. We define the scalar product as

$$\langle \mathbf{C}, \mathbf{D} \rangle = \int_{\partial\Omega} \mathbf{C}^*(\mathbf{r}) \cdot \mathbf{D}(\mathbf{r}) dS, \quad (1)$$

and the norm $\|\mathbf{C}\| = \sqrt{\langle \mathbf{C}, \mathbf{C} \rangle}$.

Any sufficiently smooth vector field \mathbf{j} defined on the surface $\partial\Omega$ can be resolved into the sum of two components: an irrotational and non-solenoidal vector field \mathbf{j}^{\parallel} and a solenoidal and rotational (non zero curl) vector field \mathbf{j}^{\perp} . This is a particular case of the Helmholtz decomposition for vector fields defined on a closed surface. The vector fields \mathbf{j}^{\parallel} and \mathbf{j}^{\perp} are orthogonal according to the above scalar product. In the following, we generate a basis for each of the two components.

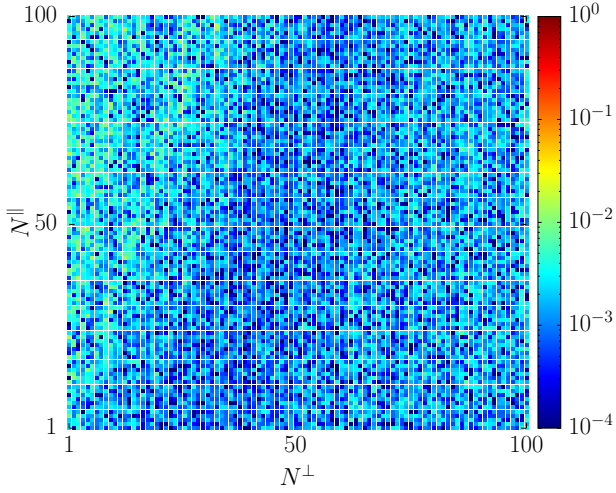


Fig. 2. “Mutual” Gram matrix $g_{h,k} = \langle \mathbf{j}_h^{\parallel}, \mathbf{j}_k^{\perp} \rangle$, which tests the orthogonality among the discrete longitudinal and transverse static modes of a sphere. The maximum occurrence of the computed Gram matrix is (in absolute value) is 0.024. Only the first 100×100 occurrences of the Gram matrix are shown.

A. Longitudinal static modes

The longitudinal static surface current modes (called in the following *longitudinal modes* for brevity) are nontrivial solutions of the eigenvalue problem:

$$\mathcal{T}_0^{\parallel} \{ \mathbf{j}_k^{\parallel} \} (\mathbf{r}) = \gamma_k^{\parallel} \mathbf{j}_k^{\parallel} \quad \text{on } \partial\Omega, \quad (2)$$

where

$$\mathcal{T}_0^{\parallel} \{ \mathbf{w} \} (\mathbf{r}) = \hat{\mathbf{n}} \times \hat{\mathbf{n}} \times \nabla \oint_{\partial\Omega} g_0(\mathbf{r} - \mathbf{r}') \nabla'_S \cdot \mathbf{w}(\mathbf{r}') dS', \quad (3)$$

being g_0 the homogeneous space static Green’s function

$$g_0(\mathbf{r} - \mathbf{r}') = \frac{1}{4\pi} \frac{1}{|\mathbf{r} - \mathbf{r}'|}. \quad (4)$$

Apart from the factor $1/\varepsilon_0$, the integral operator 3 gives the tangential component of the static electric field generated by a surface charge density distribution $(\nabla'_S \cdot \mathbf{w})$. Its spectrum has the following properties:

- i the eigenvalues $\{\gamma_k^{\parallel}\}$ and the modes $\{\mathbf{j}_k^{\parallel}\}$ depend on the shape of the object, but are independent of the object material (assumed to be homogeneous), and the frequency of operation;
- ii the eigenvalues are real and positive;
- iii the eigenmodes are orthogonal according to the scalar product 1;
- iv for a spherical surface of unit radius the eigenvalues have analytical expression

$$\frac{1}{\gamma_k^{\parallel}} = \frac{(2k+1)}{k(k+1)} \quad k = 1, 2, 3, \dots \quad (5)$$

In the following, we employ the set $\{\mathbf{j}_k^{\parallel}\}$ for the representation of square integrable solenoidal vector fields defined on $\partial\Omega$ with zero surface curl.

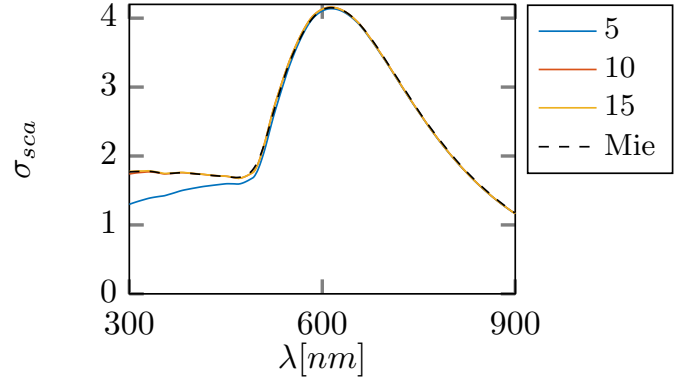


Fig. 3. Scattering efficiency σ_{sca} of a gold sphere with radius $R = 100\text{nm}$ excited by a linearly polarized plane wave in the visible and near infrared spectral range. σ_{sca} is evaluated using the PMCHWT and employing an increasing number of longitudinal and transverse static modes ($N^{\parallel} = N^{\perp} = 5, 10, 15$). The reference Mie solution (black dashed line) is also shown for comparison.

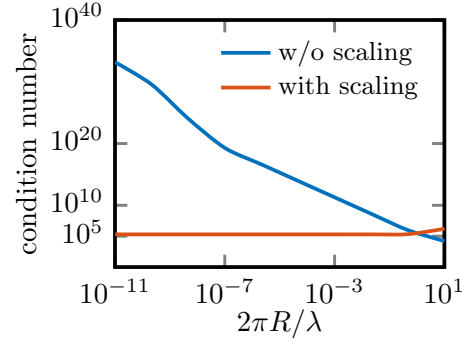


Fig. 4. Condition number with and without basis rearrangement and scaling, as a function of the size parameter $2\pi R/\lambda$, assuming $N^{\parallel} = N^{\perp} = 15$. We considered a gold sphere.

B. Transverse static modes

The transverse static surface current modes (called *transverse modes* in the following for brevity) are non trivial solutions of the eigenvalue problem:

$$\mathcal{T}_0^{\perp} \{ \mathbf{j}_k^{\perp} \} (\mathbf{r}) = \gamma_k^{\perp} \mathbf{j}_k^{\perp} \quad \text{on } \partial\Omega, \quad (6)$$

with

$$\mathcal{T}_0^{\perp} \{ \mathbf{w} \} (\mathbf{r}) = -\hat{\mathbf{n}} \times \hat{\mathbf{n}} \times \oint_{\partial\Omega} g_0(\mathbf{r} - \mathbf{r}') \mathbf{w}(\mathbf{r}') dS'. \quad (7)$$

Apart from the factor μ_0 , the integral operator 7 gives the static vector potential generated by a surface current distribution. Its spectrum has the following properties:

- i The eigenvalues $\{\gamma_k^{\perp}\}$ and the modes $\{\mathbf{j}_k^{\perp}\}$ depend on the shape of the object, and are independent of the object material (assumed to be homogeneous) and the frequency of operation
- ii the eigenvalues are real and positive;
- iii the modes $\{\mathbf{j}_k^{\perp}\}$ are orthogonal according to the scalar product 1;

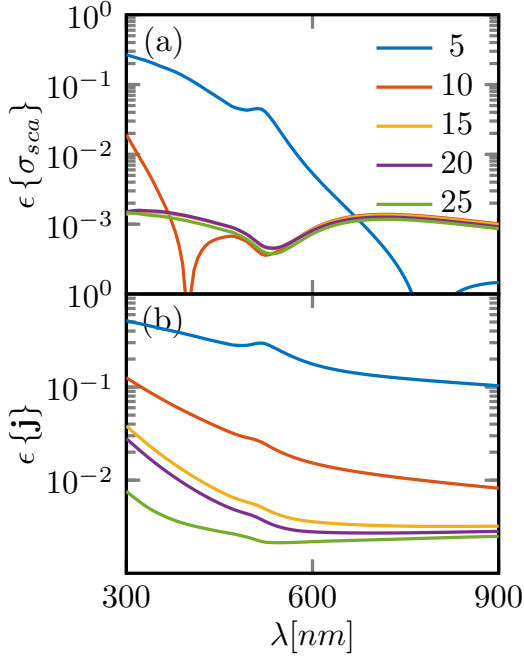


Fig. 5. Error made in the evaluation of the scattering efficiency $\epsilon\{\sigma_{sca}\}$ (a) and of the equivalent surface currents $\epsilon\{\mathbf{j}\}$ (b) obtained in the scattering from a gold sphere $R = 100\text{nm}$ by using $N^{\parallel} = N^{\perp} = 5, 10, 15, 20, 25$ static modes (20, 40, 60 degrees of freedom) against corresponding quantities evaluated by using the finite element method with 999 loop and 1996 star functions (5998 degrees of freedom). In both cases a PMCHWT formulation is used. The sphere is excited by a linearly polarized plane wave as a function of the wavelength λ .

iv for a spherical surface of unit radius the eigenvalues have analytical expression

$$\frac{1}{\gamma_k^{\perp}} = (2k + 1) \quad k = 1, 2, 3, \dots \quad (8)$$

In the following, we employ the set $\{\mathbf{j}_k^{\perp}\}$ for the representation of square integrable vector fields defined on Ω with zero surface divergence.

C. Computation of the static surface modes

Let us introduce a surface triangulation of $\partial\Omega$, with N_n vertices (nodes) and N_t elements, and N_e edges. We preliminarily compute the longitudinal and transverse static modes associated with the assigned object shape. We represent them in term of convenient low level (sub-domain) basis functions, namely loop and star basis functions [13], [36]. Specifically, any transverse mode \mathbf{j}_h^{\perp} is expanded in terms of (solenoidal) loop basis functions $\{\mathbf{j}_q^{\circ}\}$ with coefficients $\alpha_{h,q}^{\perp\circ}$. Dually, any longitudinal mode \mathbf{j}_h^{\parallel} is expanded in terms of star basis functions $\{\mathbf{j}_p^{\star}\}$ with coefficients $\alpha_{h,p}^{\parallel\star}$:

$$\mathbf{j}_h^{\parallel} = \sum_{p=1}^{N_t-1} \alpha_{h,p}^{\parallel\star} \mathbf{j}_p^{\star}, \quad \mathbf{j}_h^{\perp} = \sum_{q=1}^{N_n-1} \alpha_{h,q}^{\perp\circ} \mathbf{j}_q^{\circ}. \quad (9)$$

Both star and loop functions also admit a linear representation in terms of rooftop (RWG) [9] basis functions. For closed surfaces with no handles, the number of linearly independent

loop functions is $N_n - 1$, while the number of linearly independent star functions is $N_t - 1$. Thus, the numerical auxiliary eigenvalue problems are respectively, for longitudinal modes

$$\mathbf{T}_0^{\parallel\star\star} \mathbf{J}_h^{\star} = \gamma_h^{\parallel} \mathbf{R}^{\star\star} \mathbf{J}_h^{\star}, \quad (10)$$

where

$$(\mathbf{T}_0^{\parallel\star\star})_{pq} = \langle \mathbf{j}_p^{\star}, \mathcal{T}_0^{\parallel} \mathbf{j}_q^{\star} \rangle, \quad (\mathbf{R}^{\star\star})_{pq} = \langle \mathbf{j}_p^{\star}, \mathbf{j}_q^{\star} \rangle,$$

and for transverse modes

$$\mathbf{T}^{\perp\circ\circ} \mathbf{J}_h^{\circ} = \gamma_h^{\perp} \mathbf{R}^{\circ\circ} \mathbf{J}_h^{\circ}, \quad (11)$$

where

$$(\mathbf{T}^{\perp\circ\circ})_{pq} = \langle \mathbf{j}_p^{\circ}, \mathcal{T}_0^{\perp} \mathbf{j}_q^{\circ} \rangle, \quad (\mathbf{R}^{\circ\circ})_{pq} = \langle \mathbf{j}_p^{\circ}, \mathbf{j}_q^{\circ} \rangle.$$

Since the loop and star functions are not orthogonal, the matrices $\mathbf{R}^{\star\star}$ and $\mathbf{R}^{\circ\circ}$ and not identity matrices, thus problems 10 and 11 are generalized eigenvalue problems.

Nevertheless, the involved matrices are real, symmetric, and positive definite. Thus, efficient numerical algorithms for the eigenvalue calculation do apply, such as the Cholesky factorization [37]. Moreover, the matrices properties also determine the orthogonality, at the discrete level, of any pair of longitudinal modes, and any pair of transverse modes.

The numerical integration of shape functions times the Green's functions or its gradient are evaluated using the techniques introduced by R. Graglia [38].

III. POGGIO-MILLER-CHANG-HARRINGTON-WU-TSAI (PMCHWT) SURFACE INTEGRAL EQUATION

Let us assume that a linear, non-magnetic, homogeneous, isotropic material occupies the three-dimensional domain Ω . The material has permittivity $\epsilon^+(\omega)$, permeability $\mu^+(\omega)$ and it is surrounded by a background medium with permittivity $\epsilon^-(\omega)$ and permeability $\mu^-(\omega)$. The object is illuminated by a time harmonic electromagnetic field $\text{Re}\{\mathbf{E}_{inc} e^{i\omega t}\}$.

The equivalent electric \mathbf{j}_e and magnetic \mathbf{j}_m surface current densities, defined on $\partial\Omega$, are solution of the following surface integral problem formulated by Poggio-Miller-Chang-Harrington-Wu-Tsai [21]:

$$\mathcal{Z} \mathbf{J} = \mathbf{F}, \quad (12)$$

where

$$\mathcal{Z} = \begin{pmatrix} \zeta^- \mathcal{T}_- + \zeta^+ \mathcal{T}_+ & \mathcal{K}_- + \mathcal{K}_+ \\ -(\mathcal{K}_- + \mathcal{K}_+) & \mathcal{T}_- / \zeta^- + \mathcal{T}_+ / \zeta^+ \end{pmatrix}, \quad (13)$$

$$\mathbf{J} = [\mathbf{j}_e, \mathbf{j}_m]^T, \quad \mathbf{F} = [\mathbf{e}_0, \mathbf{h}_0]^T, \quad (14)$$

$$\mathbf{e}_0 = -\hat{\mathbf{n}} \times \hat{\mathbf{n}} \times \mathbf{E}_{inc}|_{\partial\Omega}, \quad \mathbf{h}_0 = -\hat{\mathbf{n}} \times \hat{\mathbf{n}} \times \mathbf{H}_{inc}|_{\partial\Omega}, \quad (15)$$

the operators \mathcal{K}_\pm and \mathcal{T}_\pm are the MFIE and EFIE integral operators:

$$\mathcal{K}_\pm \{\mathbf{w}\}(\mathbf{r}) = \hat{\mathbf{n}} \times \hat{\mathbf{n}} \times \int_{\partial\Omega} \mathbf{w}(\mathbf{r}') \times \nabla' g^\pm(\mathbf{r} - \mathbf{r}') dS', \quad (16a)$$

$$\begin{aligned} \mathcal{T}_\pm \{\mathbf{w}\}(\mathbf{r}) &= jk^\pm \hat{\mathbf{n}} \times \hat{\mathbf{n}} \times \int_{\partial\Omega} g^\pm(\mathbf{r} - \mathbf{r}') \mathbf{w}(\mathbf{r}') dS' \\ &+ \frac{1}{jk^\pm} \hat{\mathbf{n}} \times \hat{\mathbf{n}} \times \int_{\partial\Omega} \nabla' g^\pm(\mathbf{r} - \mathbf{r}') \nabla'_S \cdot \mathbf{w}(\mathbf{r}') dS', \end{aligned} \quad (16b)$$

$\nabla'_S \cdot$ denotes the surface divergence, g^\pm is the homogeneous space Green's function of the region Ω_\pm , i.e.

$$g^\pm(\mathbf{r} - \mathbf{r}') = \frac{e^{-jk^\pm |\mathbf{r} - \mathbf{r}'|}}{4\pi |\mathbf{r} - \mathbf{r}'|}, \quad (17)$$

$k^\pm = \omega \sqrt{\mu^\pm \varepsilon^\pm}$, and $\zeta^\pm = \sqrt{\mu^\pm / \varepsilon^\pm}$.

We anticipate that the choice of static surface modes as a basis regularizes the scattering operators, leading to an effective way to diagonalize the block-diagonal operators of the impedance matrix which are associated with the static Green function.

A. Galerkin equations

Aiming at the solution of the PMCWHT equation 12, we represent the equivalent electric and magnetic surface currents in term of the transverse static modes $\{\mathbf{j}_p^\perp\}_{p=1\dots N^\perp}$ associated to the first N^\perp eigenvalues γ_p^\perp (sorted in descending order), and in terms of the longitudinal static modes $\{\mathbf{j}_q^\parallel\}_{q=1\dots N^\parallel}$ associated with the first N^\parallel eigenvalues γ_q^\parallel (sorted in ascending order), namely

$$\begin{cases} \mathbf{j}_e(\mathbf{r}) \approx \sum_{p=1}^{N^\perp} \alpha_p^\perp \mathbf{j}_p^\perp(\mathbf{r}) + \sum_{q=1}^{N^\parallel} \alpha_q^\parallel \mathbf{j}_q^\parallel(\mathbf{r}), \\ \mathbf{j}_m(\mathbf{r}) \approx \sum_{p=1}^{N^\perp} \beta_p^\perp \mathbf{j}_p^\perp(\mathbf{r}) + \sum_{q=1}^{N^\parallel} \beta_q^\parallel \mathbf{j}_q^\parallel(\mathbf{r}). \end{cases} \quad (18)$$

Thus, N^\parallel and N^\perp are the number of longitudinal and transverse modes employed in the expansion. Therefore, we define the unknown block vectors

$$\mathbf{J}_e = \left(\boldsymbol{\alpha}^\perp | \boldsymbol{\alpha}^\parallel \right)^T, \quad \mathbf{J}_m = \left(\boldsymbol{\beta}^\perp | \boldsymbol{\beta}^\parallel \right)^T \quad (19)$$

with

$$\left(\boldsymbol{\alpha}^a \right)_p = \alpha_p^a \quad p = 1 \dots N^a, \quad \left(\boldsymbol{\beta}^a \right)_q = \beta_q^a \quad q = 1 \dots N^a, \quad (20)$$

with $a = \parallel, \perp$

We find the finite dimensional approximation of the PMCHWT problem by substituting Eq. 18 in Eq. 12 and by projecting along the same set of modes, accordingly to a Galerkin projection scheme. Eventually, we obtain:

$$\mathbf{Z}\mathbf{J} = \begin{pmatrix} \mathbf{E}_0 \\ \mathbf{H}_0 \end{pmatrix}, \quad (21)$$

where

$$\mathbf{J} = \begin{pmatrix} \mathbf{J}_e \\ \mathbf{J}_m \end{pmatrix}, \quad (22)$$

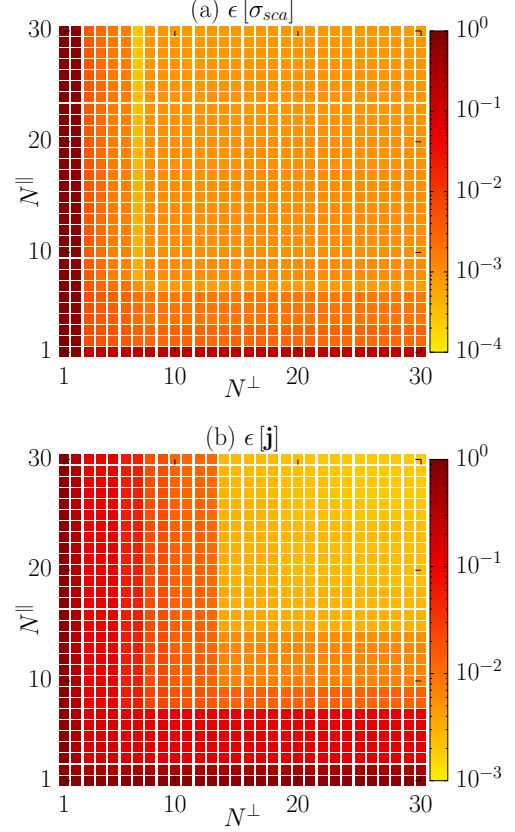


Fig. 6. Error in the evaluation of the scattering efficiency $\epsilon[\sigma_{sca}]$ (a) and of the equivalent surface currents $\epsilon[\mathbf{j}]$ (b) of the solution of the scattering problem from a gold sphere $R = 100\text{nm}$ obtained by using an entire-domain basis constituted by N^\parallel longitudinal function and N^\perp transverse function against corresponding quantities evaluated by using the finite element method with 999 loop and 1996 star functions (5998 degrees of freedom). In both cases a PMCHWT formulation is used. The sphere is excited by a linearly polarized plane wave at 620nm.

$$\mathbf{Z} = \begin{pmatrix} \zeta^- \mathbf{T}_- + \zeta^+ \mathbf{T}_+ & \mathbf{K}_- + \mathbf{K}_+ \\ -(\mathbf{K}_- + \mathbf{K}_+) & \mathbf{T}_- / \zeta^- + \mathbf{T}_+ / \zeta^+ \end{pmatrix}, \quad (23)$$

$$\mathbf{T}_\pm = \begin{pmatrix} \mathbf{T}_\pm^{\perp, \perp} & \mathbf{T}_\pm^{\perp, \parallel} \\ \mathbf{T}_\pm^{\parallel, \perp} & \mathbf{T}_\pm^{\parallel, \parallel} \end{pmatrix}, \quad \mathbf{K}_\pm = \begin{pmatrix} \mathbf{K}_\pm^{\perp, \perp} & \mathbf{K}_\pm^{\perp, \parallel} \\ \mathbf{K}_\pm^{\parallel, \perp} & \mathbf{K}_\pm^{\parallel, \parallel} \end{pmatrix}, \quad (24)$$

$$\left(\mathbf{K}_\pm^{ab} \right)_{pq} = \langle \mathbf{j}_p^a | \mathbf{K}_\pm | \mathbf{j}_q^b \rangle, \quad \left(\mathbf{T}_\pm^{ab} \right)_{pq} = \langle \mathbf{j}_p^a | \mathcal{T}_\pm | \mathbf{j}_q^b \rangle, \quad (25)$$

$$\mathbf{E}_0 = \left(\mathbf{E}_0^\perp | \mathbf{E}_0^\parallel \right)^T, \quad \mathbf{H}_0 = \left(\mathbf{H}_0^\perp | \mathbf{H}_0^\parallel \right)^T, \quad (26)$$

and

$$\left(\mathbf{E}_0^a \right)_p = \langle \mathbf{j}_p^a, \mathbf{e}_0 \rangle \quad \left(\mathbf{H}_0^a \right)_p = \langle \mathbf{j}_p^a, \mathbf{h}_0 \rangle. \quad (27)$$

with $a, b = \parallel, \perp$. In conclusion, the finite dimensional system has $2(N^\parallel + N^\perp)$ degrees of freedom.

B. Green function decomposition

We now decompose the Green function as the sum of the static Green g_0 function and a regular difference term $g_{d\pm}$:

$$g_\pm(\mathbf{r} - \mathbf{r}') = g_0(\mathbf{r} - \mathbf{r}') + g_{d\pm}(\mathbf{r} - \mathbf{r}'), \quad (28)$$

where

$$g_{d\pm}(\mathbf{r} - \mathbf{r}') = \frac{e^{-j\frac{k^\pm}{2}|\mathbf{r}-\mathbf{r}'|}}{4\pi j} k^\pm \text{sinc}\left\{\frac{k^\pm}{2}|\mathbf{r}-\mathbf{r}'|\right\}. \quad (29)$$

By applying this decomposition to the operators \mathcal{T}_\pm and \mathcal{K}_\pm , defined in 16a and 16b, we obtain:

$$\begin{aligned} \mathcal{T}_\pm &= +\frac{1}{jk^\pm} \mathcal{T}_0^\parallel - jk^\pm \mathcal{T}_0^\perp + \mathcal{T}_{d\pm}, \\ \mathcal{K}_\pm &= \mathcal{K}_0 + \mathcal{K}_{d\pm}, \end{aligned} \quad (30)$$

where \mathcal{T}_0^\parallel and \mathcal{T}_0^\perp are the static operators defined in Eqs. 3 and 7, and

$$\begin{aligned} \mathcal{T}_{d\pm}\{\mathbf{w}\}(\mathbf{r}) &= jk^\pm \hat{\mathbf{n}} \times \hat{\mathbf{n}} \times \int_{\partial\Omega} g_{d\pm}(\mathbf{r} - \mathbf{r}') \mathbf{w}(\mathbf{r}') dS' \\ &\quad - \frac{1}{jk^\pm} \hat{\mathbf{n}} \times \hat{\mathbf{n}} \times \int_{\partial\Omega} \nabla g_{d\pm}(\mathbf{r} - \mathbf{r}') \nabla'_S \cdot \mathbf{w}(\mathbf{r}') dS', \end{aligned} \quad (31)$$

$$\mathcal{K}_0\{\mathbf{w}\}(\mathbf{r}) = \hat{\mathbf{n}} \times \hat{\mathbf{n}} \times \int_{\partial\Omega} \mathbf{w}(\mathbf{r}') \times \nabla'_S g_0(\mathbf{r} - \mathbf{r}') dS', \quad (32)$$

$$\mathcal{K}_{d\pm}\{\mathbf{w}\}(\mathbf{r}) = \hat{\mathbf{n}} \times \hat{\mathbf{n}} \times \int_{\partial\Omega} \mathbf{w}(\mathbf{r}') \times \nabla'_S g_{d\pm}(\mathbf{r} - \mathbf{r}') dS'. \quad (33)$$

The above decomposition considerably simplifies the calculation of the finite dimensional operators $\mathbf{T}_\pm^{a,b}$ with $a, b = \parallel, \perp$, which are obtained by projecting the operator \mathcal{T}_\pm along the longitudinal and transverse static modes because \mathbf{j}_k^\parallel and \mathbf{j}_k^\perp diagonalize the static operators \mathcal{T}_0^\perp and \mathcal{T}_0^\parallel :

$$\begin{aligned} (\mathbf{T}_\pm^\parallel)_{pq} &= \langle \mathbf{j}_p^\parallel, \mathcal{T}_\pm \mathbf{j}_q^\parallel \rangle = \\ &\quad \frac{\gamma_p^\parallel}{jk^\pm} \delta_{p,q} - jk^\pm \langle \mathbf{j}_p^\parallel, \mathcal{T}_0^\perp \mathbf{j}_q^\parallel \rangle + \langle \mathbf{j}_p^\parallel, \mathcal{T}_{d\pm} \mathbf{j}_q^\parallel \rangle, \end{aligned} \quad (34a)$$

$$(\mathbf{T}_\pm^\perp)_{pq} = \langle \mathbf{j}_p^\perp, \mathcal{T}_\pm \mathbf{j}_q^\perp \rangle = \langle \mathbf{j}_p^\perp, \mathcal{T}_{d\pm} \mathbf{j}_q^\perp \rangle, \quad (34b)$$

$$(\mathbf{T}_\pm^\perp)_{pq} = \langle \mathbf{j}_p^\parallel, \mathcal{T}_\pm \mathbf{j}_q^\perp \rangle = \langle \mathbf{j}_p^\parallel, \mathcal{T}_{d\pm} \mathbf{j}_q^\perp \rangle, \quad (34c)$$

$$(\mathbf{T}_\pm^\perp)_{pq} = \langle \mathbf{j}_p^\perp, \mathcal{T}_\pm \mathbf{j}_q^\perp \rangle = -jk^\pm \gamma_h^\perp \delta_{p,q} + \langle \mathbf{j}_p^\perp, \mathcal{T}_{d\pm} \mathbf{j}_q^\perp \rangle, \quad (34d)$$

where $\delta_{p,q}$ is the Kronecker delta. We point out that the numerical computation of the terms $\langle \mathbf{j}_p^\parallel, \mathcal{T}_{d\pm} \mathbf{j}_q^\perp \rangle$ is straightforward, since their kernels are regular functions. These terms are the only ones depending on the operating frequency. The decomposition of the Green function into the sum of a static term and of a regular difference term relieves us from the task of computing almost all the integrals with (integrable) singularity, which usually results in longer computational time compared to their regular counterpart. There are however two exceptions: $\langle \mathbf{j}_p^\parallel, \mathcal{T}_0^\perp \mathbf{j}_q^\parallel \rangle$ and $\langle \mathbf{j}_p^\perp, \mathcal{K}_0^\perp \mathbf{j}_q^\perp \rangle$, $\forall a, b \in \perp, \parallel$. These terms are frequency-independent, thus when the calculation of the scattering response of an object for multiple frequencies of the exciting field is required, they can be conveniently precalculated and stored away, while only the regular terms must be calculated at any frequencies.

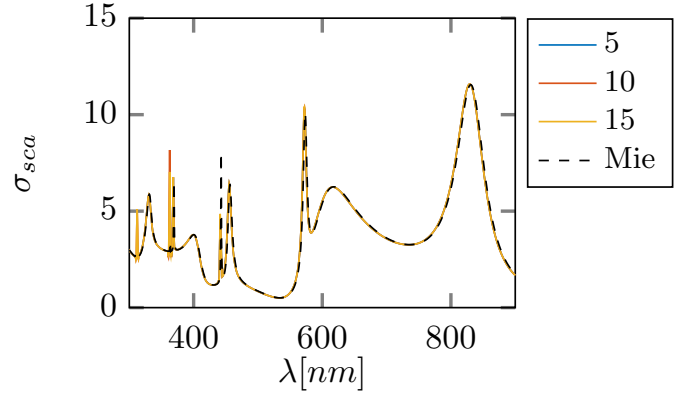


Fig. 7. Scattering efficiency σ_{sca} of a silicon object with $R = 100\text{nm}$ excited by a linearly polarized plane wave in the visible spectral range evaluated by the PMCHWT with a static basis with an increasing number of longitudinal and transverse static modes with $N^\parallel = N^\perp = 5, 10, 15$. The reference Mie solution (black dashed line) is also shown for comparison.

C. Low-frequency analysis

Surface integral formulations may suffer from ill-conditioning due to low frequency breakdown. The low frequency breakdown phenomenon manifests when the operating wavelength is much larger than the dimension of the object [39], and originates from the different frequency-scaling of the terms associated with the vector and the scalar potentials. This is a common scenario which may be encountered in several applications, including metamaterials and electromagnetic bandgap (EBG) structures, or in the analysis of interconnects and packaging. This problem has been addressed by using quasi-Helmholtz decompositions, such as loop-star [39], [36], [40], loop-tree [14], [41], or null-pinv [42] decomposition, followed by a basis rearrangement [43], [44]. It is also worth to point out that some formulations are immune to this problem, such as the N-Müller formulation [45], or the formulation obtained by augmenting the traditional EFIE by including charge as extra unknown [46], [47].

In this section, we summarize the behaviour of the PMCHWT at very low frequencies. In this limit, the frequency dependence of the elements of the matrix Z follows different scaling laws, which are easily determined by following Ref. [44]

$$\begin{pmatrix} \mathbf{T}_\pm^{\perp\perp} & \mathbf{T}_\pm^{\parallel\perp} \\ \mathbf{T}_\pm^{\perp\parallel} & \mathbf{T}_\pm^{\parallel\parallel} \end{pmatrix} \xrightarrow{\omega \downarrow 0} \begin{pmatrix} -jk^\pm \Gamma^\perp & j(k^\pm)^3 \mathbf{T}_2^{\parallel\perp} \\ j(k^\pm)^3 \mathbf{T}_2^{\perp\parallel} & +\Gamma^\parallel / jk^\pm \end{pmatrix} \quad (35)$$

$$\begin{pmatrix} \mathbf{K}_\pm^{\perp\perp} & \mathbf{K}_\pm^{\perp\parallel} \\ \mathbf{K}_\pm^{\parallel\perp} & \mathbf{K}_\pm^{\parallel\parallel} \end{pmatrix} \xrightarrow{\omega \downarrow 0} \begin{pmatrix} (k^\pm)^2 \mathbf{K}_2^{\perp\perp} & \mathbf{K}_0^{\perp\perp} \\ \mathbf{K}_0^{\perp\parallel} & \mathbf{K}_0^{\parallel\parallel} \end{pmatrix} \quad (36)$$

where Γ^\perp and Γ^\parallel are diagonal matrices,

$$\begin{aligned} \Gamma^\perp &= \text{diag}\{\gamma_1^\perp, \gamma_2^\perp, \dots, \gamma_{N^\perp}^\perp\}, \\ \Gamma^\parallel &= \text{diag}\{\gamma_1^\parallel, \gamma_2^\parallel, \dots, \gamma_{N^\parallel}^\parallel\}, \end{aligned} \quad (37)$$

and

$$\begin{aligned} T_2^{\perp\perp} &= \frac{1}{8\pi} \int_{\partial\Omega} \mathbf{j}_p^\perp(\mathbf{r}) \cdot \int_{\partial\Omega} |\mathbf{r} - \mathbf{r}'| \mathbf{j}_q^\perp(\mathbf{r}') dS dS', \quad (38) \\ K_2^{\perp\perp} &= -\frac{1}{8\pi} \int_{\partial\Omega} \mathbf{j}_p^\perp(\mathbf{r}) \cdot \int_{\partial\Omega} \frac{(\mathbf{r} - \mathbf{r}')}{|\mathbf{r} - \mathbf{r}'|} \times \mathbf{j}_q^\perp(\mathbf{r}') dS dS' \end{aligned} \quad (39)$$

Thus, by using Eqs. 35-36 it easy to prove that, in the static limit, the discrete matrix \mathbf{Z} approaches the matrix \mathbf{Z}_0 which exhibits the following frequency dependence:

$$\mathbf{Z}_0 \propto \begin{bmatrix} \mathcal{O}(\omega) & \mathcal{O}(\omega^3) & \mathcal{O}(\omega^2) & \mathcal{O}(1) \\ \mathcal{O}(\omega^3) & \mathcal{O}(\omega^{-1}) & \mathcal{O}(1) & \mathcal{O}(1) \\ \mathcal{O}(\omega^2) & \mathcal{O}(1) & \mathcal{O}(\omega) & \mathcal{O}(\omega^3) \\ \mathcal{O}(1) & \mathcal{O}(1) & \mathcal{O}(\omega^3) & \mathcal{O}(\omega^{-1}) \end{bmatrix} \quad (40)$$

The excitation vector associated with a plane wave exhibits the following dependencies [44]:

$$\begin{pmatrix} E_0^\perp \\ E_0^\parallel \\ H_0^\perp \\ H_0^\parallel \end{pmatrix} \propto \begin{pmatrix} \mathcal{O}(k_0) \\ \mathcal{O}(1) \\ \mathcal{O}(k_0) \\ \mathcal{O}(1) \end{pmatrix}. \quad (41)$$

Following [44], we introduce the rearrangement and scaling of the basis

$$\tilde{\mathbf{Z}} = \mathbf{D}_1 \mathbf{Z} \mathbf{D}_2, \quad (42)$$

where

$$\begin{aligned} \mathbf{D}_1 &= \text{diag} \{ k_-^{-1} \mathbf{I}_{N^\perp}, \mathbf{I}_{N^\parallel}, k_-^{-1} \mathbf{I}_{N^\perp}, \mathbf{I}_{N^\parallel} \}, \\ \mathbf{D}_2 &= \text{diag} \{ \mathbf{I}_{N^\perp}, ik_- \mathbf{I}_{N^\parallel}, \mathbf{I}_{N^\perp}, ik_- \mathbf{I}_{N^\parallel} \}. \end{aligned} \quad (43)$$

where \mathbf{I}_{N^\perp} is the the $N^\perp \times N^\perp$ identity matrix, and \mathbf{I}_{N^\parallel} is the $N^\parallel \times N^\parallel$ identity matrix. After the above rearrangement the matrix $\tilde{\mathbf{Z}}$ is well-behaved.

IV. RESULTS AND DISCUSSION

We introduce a triangular surface mesh for $\partial\Omega$ with N_n nodes and N_t triangular elements, then we precompute the longitudinal and static modes of a sphere, using $N^* = N_t - 1$ star and $N^\circ = N_n - 1$ loop functions respectively, by solving the eigenvalue problems 10 and 11. We assembly a finite-dimensional basis by only considering the static modes associated to the first N^\parallel longitudinal eigenvalues (sorted in ascending order) and to the first N^\perp transverse eigenvalues (sorted in descending order). The discrete PMCHWT impedance matrix \mathbf{Z} is then assembled, where static part of the operators lying on the block-diagonal are diagonalized as shown in Eqs. 34. The resulting complex and non-hermitian matrix has dimension $2(N^\parallel + N^\perp)$ and it is inverted by LU decomposition (unless explicitly stated), once the excitation conditions are assigned.

A. Scattering from a sphere

We first consider the scattering from a sphere, which have an analytical solution [48], [18] and also analytical expression for the eigenvalues and for the static modes [26].

1) *Generation of the static basis:* Figure 1 shows the convergence of the eigenvalues $\{\gamma_h^\parallel\}$ and $\{\gamma_h^\perp\}$ against their analytical counterpart as a function of the triangular mesh density. The convergence is good. From now on, we consider the static basis calculated using a triangular mesh with $N_n = 1000$, $N_t = 1996$. Thus, the longitudinal static modes are represented in terms of $N_t - 1 = 1995$ star functions, while the transverse static modes are represented by $N_p - 1 = 999$ loop functions.

2) *Numerical Orthogonality and Gram matrices:* In the discrete problem, the orthogonality between any pair of longitudinal modes and between any pair of transverse modes is always guaranteed, because the matrices $T^{\circ\circ}$ and T^{**} are real and symmetric. This property is indeed verified at the numerical level with machine precision. Instead, even if we expect that the mutual product between a transverse and a longitudinal static mode to be vanishing, this fact is only approximately verified, since the sub-domain basis functions used to represent the longitudinal modes are no rigorously curl-free [40]. Thus, it is worth calculating the ‘‘mutual’’ Gram matrix G , whose occurrences are defined as

$$g_{hk} = \langle \mathbf{j}_h^\perp, \mathbf{j}_k^\parallel \rangle \quad (44)$$

The maximum occurrence of the mutual Gram matrix is 0.024, for a sphere with the considered surface mesh. In Fig. 2 are reported the first 100×100 occurrences of the Gram Matrix.

3) *Gold sphere:* We now use the static modes to solve the scattering problem from a gold sphere of radius $R = 100\text{nm}$ in the visible and near infrared spectral range [300, 900]nm. At these frequencies, a metal sphere may undergo plasmonic resonances, which have an electrostatic origin [27]. We describe the gold permittivity by interpolating experimental data [49]. The sphere is excited by a linearly polarized plane wave. We solve the PMCHWT by varying the numbers N^\parallel and N^\perp of employed longitudinal and transverse static modes, respectively.

Figure 3 shows the scattering efficiency σ_{sca} as a function of the wavelength of the exciting plane wave. The scattering efficiency is defined as the scattering cross section normalized by the geometrical cross section G which, in this case, is $G = \pi R^2$ [18]. We consider different solutions, obtained by increasing the number of modes employed in the expansion 18, i.e. $N^\parallel = N^\perp = 5, 10, 15$. The reference Mie solution [18] (black dashed line) is also shown for comparison. For $N^\parallel = N^\perp = 5$, the numerical solution is in good agreement with the reference solution only in the long-wavelength regime, while it shows a slight disagreement when the operating wavelength becomes comparable with the sphere’s radius. Increasing the number of modes to $N^\parallel = N^\perp = 10$, we obtain a good agreement over the whole investigated spectrum. In this latter case, the inversion of a 40×40 matrix is required (at each frequency).

In Fig. 4, we show the condition number of the PMCHWT problem with and without the rearrangement of the basis described in section III-C as a function of the sphere radius R , while the wavelength of the exciting plane wave is kept constant to 620nm. It is apparent that, without the basis rearrangement, the condition number exponentially increases,

which is symptomatic of the low-frequency breakdown problem. By rearranging the basis, the condition number is constant over the whole investigated range of size parameters.

We now present a more systematic analysis of the error. In particular, we define the relative error on the scattering efficiency

$$\epsilon[\sigma_{sca}] = |\sigma_{sca} - \tilde{\sigma}_{sca}| / \tilde{\sigma}_{sca}, \quad (45)$$

where $\tilde{\sigma}_{sca}$ is the reference solution which computed by solving the PMCHWT problem applying the finite element method with $N^\circ = 999$ loop functions and $N^* = 1995$ star functions, associated with the same mesh used for the static modes generation, which correspond to 5998 degrees of freedom. In Fig. 5 (a) we plot $\epsilon[\sigma_{sca}]$ as a function of the wavelength of the incident field, by varying the number of modes $N^\parallel = N^\perp$. We note that for $N^\parallel = N^\perp \geq 10$ the achieved error is lower than 0.002 all over the investigated spectral range. The error does not appreciably decrease if the number of modes $N^\parallel = N^\perp$ is increased from 15 to 25. Then, we investigate the error in the evaluation of the equivalent surface currents induced on $\partial\Omega$, which are the unknowns of the PMCHWT problem. They are immediately related to the total electric field on the surface of the object, which has a great importance in nano-optics applications [50]. We define this relative error as:

$$\epsilon[\mathbf{J}] = \|\mathbf{J} - \tilde{\mathbf{J}}\|_2 / \|\tilde{\mathbf{J}}\|_2, \quad (46)$$

where $\tilde{\mathbf{J}}$ is the reference loop/star solutions and $\|\cdot\|_2$ is the Euclidean norm. In Fig. 5 (b), we show the quantity $\epsilon[\mathbf{J}]$ as a function of the wavelength. Compared to panel (a), it is apparent that more static basis functions are needed to reach smaller errors. Also in this case, we observe a saturation of the error.

We further delve into error analysis by monitoring in Fig. 6 the same two relative errors $\epsilon[\sigma_{sca}]$ and $\epsilon[\mathbf{j}]$, by *independently* varying the number of employed modes N^\parallel and N^\perp . This analysis is carried out in correspondence of the σ_{sca} peak (see Fig. 3) occurring at $\lambda = 620\text{nm}$. The two colormaps are almost symmetric (along the principal diagonal): This fact suggests that for practical applications is convenient to keep $N^\parallel = N^\perp$. Figure 6 (a) shows that it is sufficient to consider $N^\parallel = N^\perp = 3$ (12 degrees of freedom in total) to achieve an error below 0.02. As in the previous analysis, given the same pair N^\parallel, N^\perp , the error $\epsilon[\mathbf{J}]$ is higher than $\epsilon[\sigma_{sca}]$. Specifically, we need to consider $N^\parallel = N^\perp = 10$ (40 degrees of freedom in total) to achieve an error $\epsilon\{\mathbf{J}\}$ below 0.02. It also apparent from the colormaps that the error undergoes sudden ‘‘jumps’’ in correspondence to specific values of the number of modes, namely, when a specific static mode (needed for a correct description of the solution) is included in the current density expansion. We also observe a *saturation* of the error level for high values of N^\parallel and N^\perp , namely an increase of the number of static basis function does not correspond to an appreciable decrease of the error.

4) *High-permittivity sphere*: We now consider a high permittivity sphere, assumed to be non-dispersive in time with relative permittivity $\epsilon_R = 16$. Sub-wavelength objects of sufficiently high permittivity - as the one under consideration

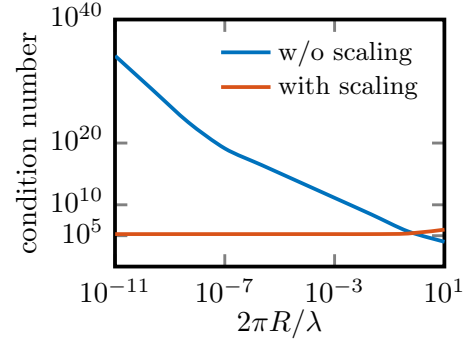


Fig. 8. Condition number with and without basis rearrangement and scaling, as a function of the size parameter $2\pi R/\lambda$, assuming $N^\parallel = N^\perp = 15$. We consider a Si sphere.

- may support magnetostatic scattering resonances [29]. These resonances arise from the interplay of the polarization energy of the dielectric and the energy stored in the magnetic field [29], [31]. This fact allows us to explore the numerical accuracy of the static basis in a complementary regime to the one of the plasmonic resonances occurring in metals.

In Fig. 7, we calculate the scattering efficiency σ_{sca} as a function of the wavelength of the exciting, linearly polarized, plane wave. We consider different solution computed using an increasing the number of modes $N^\parallel = N^\perp$. We use as reference the analytic Mie solution [48], [18], shown with a black dashed line. For $N^\parallel = N^\perp = 5$, even if a good agreement is found at low frequency, the accuracy of the solution rapidly deteriorates at higher frequencies, and it is unable to describe some peaks of the scattering response. By increasing the number of employed modes to $N^\parallel = N^\perp = 10$, we obtain a very good agreement over the whole investigated spectrum.

In Fig. 8, we show the condition number of the PMCHWT problem with and without the rearrangement of the basis described in section III-C as a function of the sphere radius R , while the wavelength of the exciting plane wave is kept constant to 620nm. As for metal sphere, by rearranging the basis, we are able to keep the condition number constant over the whole investigated range of radii.

We now quantify the errors in the scattering efficiency and in the surface currents made by solution in terms of static modes. In Fig. 9 (a) we plot $\epsilon[\sigma_{sca}]$ as a function of the incident wavelength, employing an increasing number of modes with the constrain $N^\perp = N^\parallel$. When $N^\perp = N^\parallel = 5$, the error is acceptable as long the incident wavelength is much larger than the dimension of the object, then the error suddenly increases for wavelengths below 600nm. By assuming $N^\perp = N^\parallel = 10$, we obtain a low error all over the investigated spectrum. Only in correspondence of the resonances the error slightly exceeds 0.01. A further increase in the number of basis function improves the convergence, especially in the neighborhood of the resonance peaks.

In Fig. 10 we investigate the error as a function of the number of longitudinal N^\parallel and transverse N^\perp modes which are now assumed as independent. This analysis is carried out at the wavelength $\lambda = 620\text{nm}$, which corresponds to the low fre-

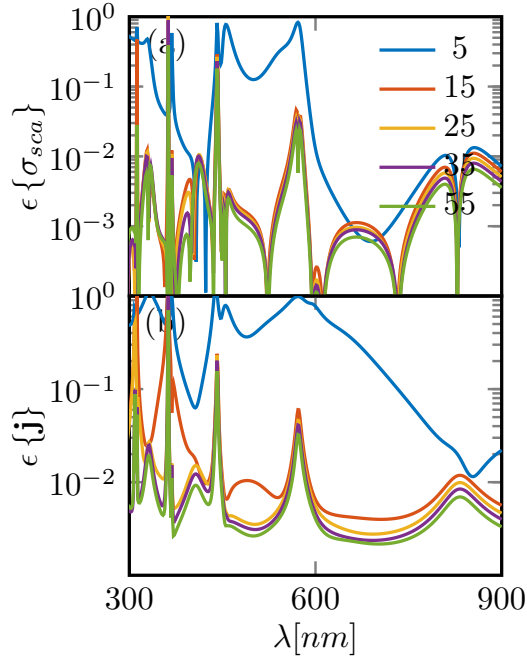


Fig. 9. Error ϵ in the evaluation of the scattering efficiency σ_{sca} (a) and of the equivalent surface currents \mathbf{j} (b) of a sphere with $\epsilon_R = 16$ and $R = 100\text{nm}$ by using an entire-domain basis constituted by $N^\parallel = N^\perp = 5, 10, 15, 25, 35, 55$ static modes. The solution evaluated by using loop/star sub-domain basis function was assumed as a reference. In both cases a PMCHWT formulation is used (5998 degrees of freedom). The sphere is excited by a linearly polarized plane wave as a function of the wavelength λ .

quency peak (first peak from the right) of the scattering cross section, where the magnetic dipole mode resonates. In Fig. 10 (a) we show the error on the scattering efficiency $\epsilon[\sigma_{sca}]$, in 10 (b) the error on the equivalent surface currents $\epsilon[\mathbf{j}]$. The two colormaps are, to a good approximation, symmetric with respect to the main diagonal. This fact suggests that for practical applications it is reasonable to choose $N^\parallel = N^\perp$. For the scattering cross section by choosing $N^\parallel = N^\perp = 3$ we reach an error below 0.01. The error in the determination of the electric and magnetic currents is in general higher, and $N^\parallel = N^\perp = 8$ are needed to achieve $\epsilon[\mathbf{j}] < 0.1$. In both panels, we observe an error saturation for large number of modes.

V. ROD

We now consider a non-canonical shape, namely a three-dimensional rod. We model this shape as a superellipsoid, whose boundary has the implicit equation

$$\left(\frac{x}{a}\right)^r + \left(\frac{y}{b}\right)^r + \left(\frac{z}{c}\right)^r = 1, \quad (47)$$

with $b = 0.5a$, $c = 0.25a$, and $r = 6$. We used the public domain code developed by Per-Olof Persson and Gilbert Strang [51] to generate a surface mesh for this implicit surface. The resulting mesh that we consider thought this section features 1000 nodes, 1996 triangular elements.

The first 16 longitudinal and 16 transverse static modes are shown in Fig. 11 and 12, respectively. The modes are shown in a lexicographic order, sorted accordingly to their static eigenvalue.

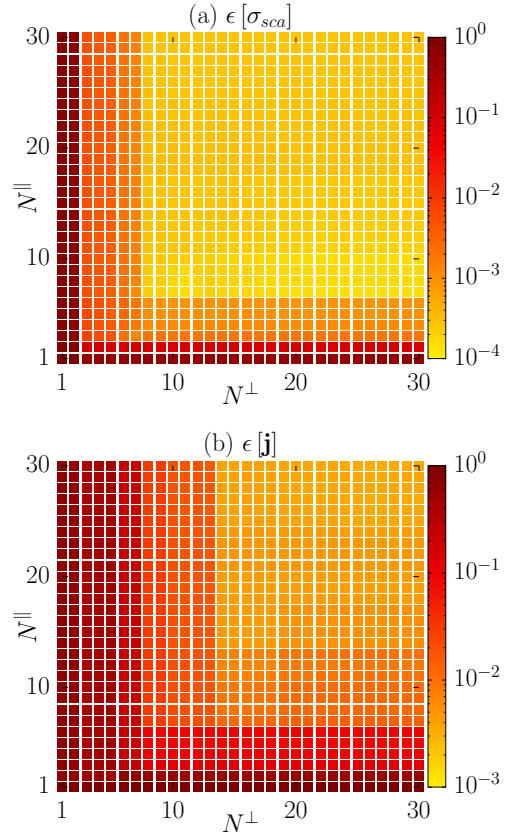


Fig. 10. Error ϵ in the evaluation of the scattering efficiency $\epsilon[\sigma_{sca}]$ (a) and of the equivalent surface currents $\epsilon[\mathbf{j}]$ (b) of the solution of the scattering problem from a sphere with $R = 100\text{nm}$ and $\epsilon_R = 16$, obtained by using an entire-domain basis constituted by N^\parallel longitudinal function and N^\perp transverse function against corresponding quantities evaluated by using the finite element method with 999 loop and 1996 star functions (5998 degrees of freedom). In both cases a PMCHWT formulation is used. The sphere is excited by a linearly polarized plane wave at 620nm.

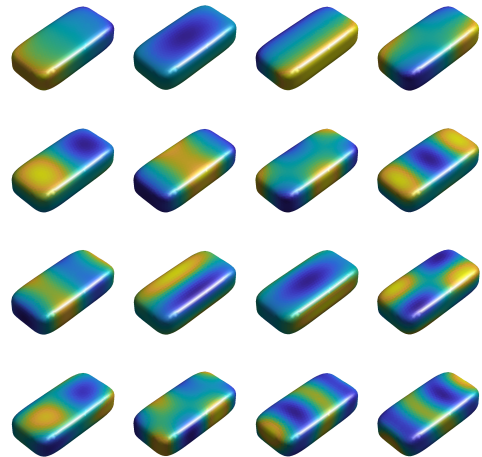


Fig. 11. Longitudinal static modes of a rod with semi-axis 1 : 0.5 : 0.25. The modes are shown in lexicographic order (ascending), sorted accordingly to their static eigenvalue. The first 16 modes are shown.

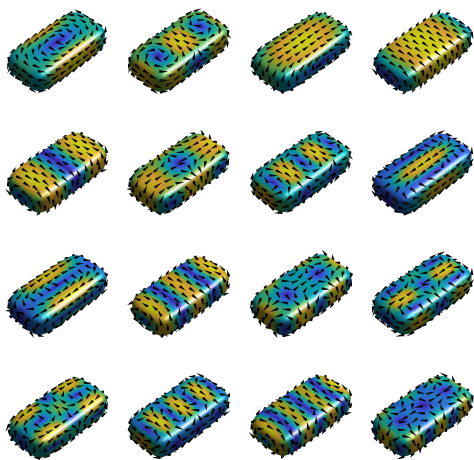


Fig. 12. Transverse static modes of a rod with semi-axis 1 : 0.5 : 0.25. The modes are shown in a lexicographic order (descending), sorted accordingly to their static eigenvalue. The first 16 modes are shown.

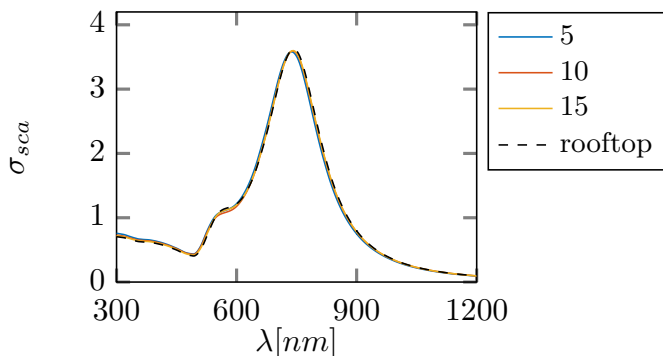


Fig. 13. Scattering efficiency σ_{sca} of gold rod with semi-axis $a = 100nm$, $b = 0.5a$, and $c = 0.25a$ evaluated with an increasing number of longitudinal and transverse static modes $N^{\perp} = N^{\parallel} = 5, 15, 25, 35, 55$. The rod is excited by a linearly polarized plane wave in the visible spectral range. The reference loop-star solution (black dashed line) is also shown for comparison.

1) *Plasmon Rod*: First, we investigate a gold rod with $a = 100nm$, excited by a plane wave linearly polarized along the direction $(\hat{x} + \hat{y})/\sqrt{2}$ and propagating along the \hat{z} axis. The gold's dispersion relation has been described using experimental data [49]. In Fig. 11 we plot the spectrum of the scattering efficiency σ_{sca} , obtained by increasing the number of modes $N^{\perp} = N^{\parallel} = 5, 10, 15$. We take as reference the finite element solution, obtained by describing the unknowns in terms of loop and star basis function, with 5984 total degrees of freedom. Only five longitudinal and transverse modes (20 total degrees of freedom) are sufficient to achieve a very good agreement with the reference solution over the whole investigated spectrum, demonstrating a drastic reduction of the total number of unknowns.

In Fig. 14, we carry out a more systematic analysis of the error (a) on the scattering cross section $\epsilon[\sigma_{sca}]$, and (b) on the equivalent surface currents $\epsilon\{j\}$. Overall, the errors are slightly higher than in the case of a sphere. Besides that, as in the previous numerical experiments, we conclude that i) the error on the surface currents are one order of magnitude higher than the error on the scattering efficiency, and ii) the different errors

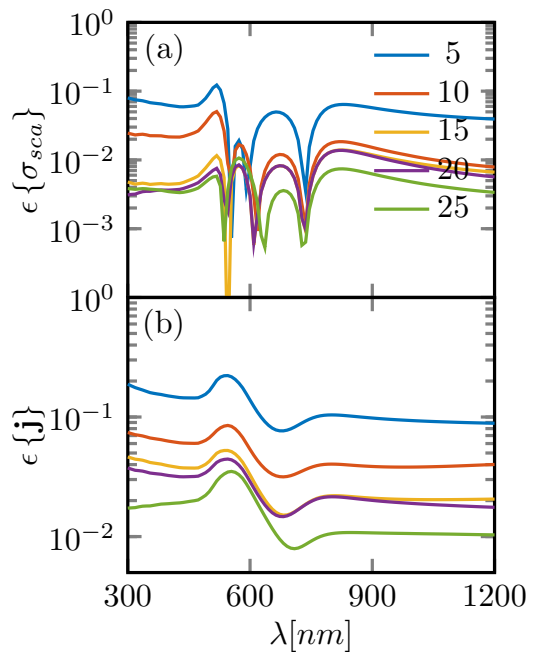


Fig. 14. Error ϵ in the evaluation of the scattering efficiency σ_{sca} and of the equivalent surface current density of a gold rod with semi-axis $a = 100nm$, $b = 0.5a$, and $c = 0.25a$ by using an increasing number of longitudinal and transverse static modes $N^{\perp} = N^{\parallel} = 5, 15, 20, 25$ ($4N^{\parallel}$ total degrees of freedom). The solution evaluated by using loop/star sub-domain basis function was assumed as a reference (5988 degrees of freedom).

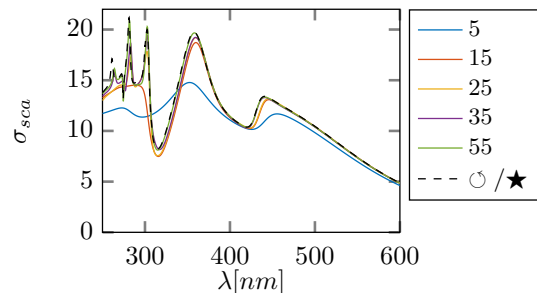


Fig. 15. Scattering efficiency σ_{sca} of dielectric rod with permittivity $\epsilon_R = 16$ and semi-axis $a = 100nm$, $b = 0.5a$, and $c = 0.25a$ evaluated with an increasing number of longitudinal and transverse static modes $N^{\perp} = N^{\parallel} = 5, 15, 25, 35, 55$. The rod is excited by a linearly polarized plane wave in the visible spectral range. The reference loop-star solution (black dashed line) is also shown for comparison (5988 degrees of freedom).

saturate if a large number of modes is employed.

2) *High-permittivity Rod*: Eventually, we investigate a high-permittivity rod. The relative permittivity of the rod is assumed constant over the investigated frequency spectrum to the value $\epsilon_R = 16$.

In Fig. 15, we plot the σ_{sca} spectrum, obtained by increasing the numbers of modes employed to expand the equivalent surface currents $N^{\perp} = N^{\parallel} = 5, 15, 35, 55$. We use as reference the finite element solution in terms of loop and star basis functions, with 5984 degrees of freedom. If the wavelength is much larger than the dimension of the rod, $N^{\perp} = N^{\parallel} = 15$ are enough to correctly describe the scattering cross section. Nevertheless, the accuracy is lost as soon as the wavelength becomes comparable to the linear dimensions of

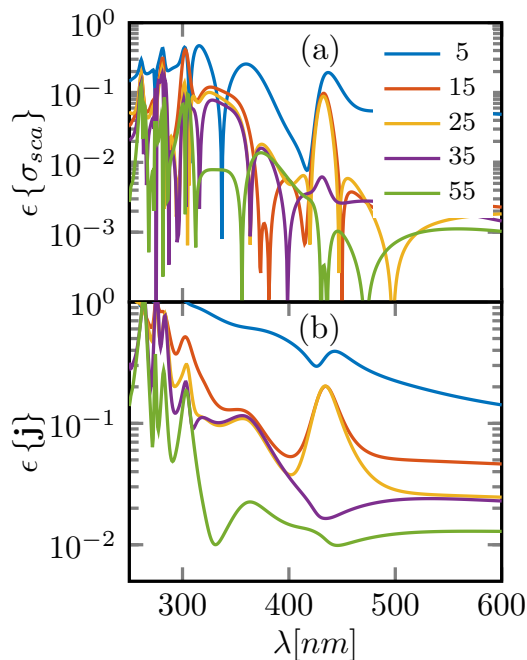


Fig. 16. Error ϵ in the evaluation of the scattering efficiency σ_{sca} and of the equivalent surface current density of a dielectric rod with permittivity $\epsilon_R = 16$ with semi-axis $a = 100nm$, $b = 0.5a$, and $c = 0.25a$ by using an increasing number of longitudinal and transverse static modes $N^\perp = N^\parallel = 5, 15, 25, 35, 55$. The solution evaluated by using loop/star basis function was assumed as a reference (5988 degrees of freedom).

the rod and high-frequency resonance peaks are not correctly described. Only by increasing the number of modes $N^\perp = N^\parallel$ to 55, all the resonance peaks, including the high-frequency ones, are correctly described.

Figure 16 offers a more quantitative analysis of the errors (a) $\epsilon[\sigma_{sca}]$, (b) $\epsilon[\mathbf{j}]$. We note that while for large wavelength a number of modes $N^\perp = N^\parallel = 15$ is sufficient to have an error below $\epsilon[\sigma_{sca}] < 0.01$ and $\epsilon[\mathbf{j}] < 0.2$, if the wavelength becomes comparable to the rod largest dimension, as many as 55 basis function are needed to contain the error. Even in this case, the accuracy is deteriorated in the neighborhood of the resonance peaks.

In conclusion, even if compared to the previously investigated scenarios, a higher number of modes is needed to correctly describe the unknown current densities, the number of modes needed to describe the solution still remains much smaller than the number of loop/star functions required to achieve a comparable accuracy.

VI. CONCLUSIONS

We investigated the use of longitudinal and transverse static modes to represent the unknowns of surface integral equations governing the electromagnetic scattering problem from penetrable objects. Longitudinal modes are constituted by the irrotational eigenmodes of the electrostatic surface integral operator, which gives the scalar potential as a function of the surface charge density. Transverse modes are constituted by the solenoidal eigenmodes of the magnetostatic surface integral operator, which returns the vector potential as a

function of the surface current distribution. These two sets are orthogonal. These modes only depends on the shape of the object, thus, the same basis can be used (and it brings the same advantages) regardless of the operating frequency and material of object. This fact enables the description of any scattering scenario involving one or more objects of a given shape, but different size, material, and spatial arrangement, in terms of the same “alphabet” of basis function, regardless of the frequency of operation.

Specifically, we demonstrate the effectiveness of the static mode expansion in the solution of the Poggio-Miller-Chang-Harrington-Wu-Tsai formulation of the electromagnetic scattering problem by a penetrable object. The choice of static basis expansion regularizes the scattering operators, leading to an effective way to diagonalize the block-diagonal operators of the impedance matrix which are associated with the static Green function. As a test case scenario, we considered the scattering from metal (plasmonic) objects and high permittivity dielectric objects, which exhibit resonances which are often challenging to model numerically. We monitor the accuracy of equivalent surface currents densities and of the scattering efficiency as the number of modes is varied. We found that, in all the investigated cases, this method drastically reduces the number of unknowns compared to discretization in terms of sub-domain functions. The minimum number of modes required to obtain a prescribed level of accuracy does depend on the shape of the object, its material, and its characteristic dimension compared to the wavelength of operation. Our numerical experiments suggest that an accurate modeling of metal penetrable objects under plane wave excitation demands for fewer static modes than high-permittivity dielectric objects. This fact is due to the multitude of dielectric resonances that the high-permittivity objects exhibit as the frequency increases. As expected, far field observables, such as the scattering efficiency, are affected by smaller errors if compared to near field observables such as the equivalent electric and magnetic currents. For all investigated scenarios, we also found a saturation of the error when a large number of static modes is employed in the expansion.

The results presented in this paper may promote the use of the static basis in multiple scattering problems, including the numerical modeling of metasurfaces and metalens.

REFERENCES

- [1] R. E. Collin, *Antennas and Radiowave Propagation*. McGraw-Hill College, 1985. [Online]. Available: https://books.google.it/books/about/Antennas_and_Radiowave_Propagation.html?id=YHepAAAACAAJ&redir_esc=y
- [2] N. Yu and F. Capasso, “Flat optics with designer metasurfaces,” *Nature Materials*, vol. 13, no. 2, pp. 139–150, Feb. 2014, bandiera_abtest: a Cg_type: Nature Research Journals Number: 2 Primary_atype: Reviews Publisher: Nature Publishing Group Subject_term: Metamaterials Subject_term_id: metamaterials. [Online]. Available: <https://www.nature.com/articles/nmat3839>
- [3] M. Khorasaninejad, F. Aieta, P. Kanhaiya, M. A. Kats, P. Genevet, D. Rousso, and F. Capasso, “Achromatic Metasurface Lens at Telecommunication Wavelengths,” *Nano Letters*, vol. 15, no. 8, pp. 5358–5362, Aug. 2015, publisher: American Chemical Society. [Online]. Available: <https://doi.org/10.1021/acs.nanolett.5b01727>
- [4] W. C. Chew, J.-M. Jin, E. Michielssen, and J. Song, Eds., *Fast and Efficient Algorithms in Computational Electromagnetics*. Boston: Artech House, July 2000.

- [5] O. M. Bucci and G. D. Massa, "Use of characteristic modes in multiple-scattering problems," *Journal of Physics D: Applied Physics*, vol. 28, no. 11, p. 2235, Nov. 1995, publisher: IOP Publishing. [Online]. Available: <https://iopscience.iop.org/article/10.1088/0022-3727/28/11/003/meta>
- [6] G. Angiulli, G. Amendola, and G. D. Massa, "Characteristic Modes in Multiple Scattering by Conducting Cylinders of Arbitrary Shape," *Electromagnetics*, vol. 18, no. 6, pp. 593–612, Nov. 1998, publisher: Taylor & Francis _eprint: <https://doi.org/10.1080/02726349808908615>. [Online]. Available: <https://doi.org/10.1080/02726349808908615>
- [7] A. Doicu, T. Wriedt, and Y. A. Eremin, *Light Scattering by Systems of Particles: Null-Field Method with Discrete Sources: Theory and Programs*, ser. Springer Series in Optical Sciences. Berlin Heidelberg: Springer-Verlag, 2006. [Online]. Available: <http://www.springer.com/gp/book/9783540336969>
- [8] B. Cockburn, G. E. Karniadakis, and C.-W. Shu, *Discontinuous Galerkin Methods: Theory, Computation and Applications*. Springer Science & Business Media, Dec. 2012, google-Books-ID: uOhrCAAQBAJ.
- [9] S. Rao, D. Wilton, and A. Glisson, "Electromagnetic scattering by surfaces of arbitrary shape," *IEEE Transactions on Antennas and Propagation*, vol. 30, no. 3, pp. 409–418, May 1982, conference Name: IEEE Transactions on Antennas and Propagation.
- [10] A. Bossavit, *Computational electromagnetism: variational formulations, complementarity, edge elements*. Academic Press, 1998.
- [11] R. Albanese and G. Rubinacci, "Integral formulation for 3D eddy-current computation using edge elements," *IEE Proceedings A (Physical Science, Measurement and Instrumentation, Management and Education, Reviews)*, vol. 135, no. 7, pp. 457–462, 1988, publisher: IET.
- [12] G. Rubinacci and A. Tamburrino, "A broadband volume integral formulation based on edge-elements for full-wave analysis of lossy interconnects," *IEEE transactions on antennas and propagation*, vol. 54, no. 10, pp. 2977–2989, 2006, publisher: IEEE.
- [13] D. Wilton, J. Lim, and S. Rao, "A novel technique to calculate the electromagnetic scattering by surfaces of arbitrary shape," *URSI Radio Science Meeting*, p. 322, 1993.
- [14] W.-L. Wu, A. W. Glisson, and D. Kajfez, "A study of two numerical solution procedures for the electric field integral equation at low frequency," *Applied Computational Electromagnetics Society Journal*, vol. 10, no. 3, pp. 69–80, 1995.
- [15] L. Trintinalia and H. Ling, "First Order Triangular Patch Basis Functions for Electromagnetic Scattering Analysis," *Journal of Electromagnetic Waves and Applications*, vol. 15, no. 11, pp. 1521–1537, Jan. 2001, publisher: Taylor & Francis _eprint: <https://doi.org/10.1163/156939301X00085>. [Online]. Available: <https://doi.org/10.1163/156939301X00085>
- [16] A. Buffa and S. H. Christiansen, "A Dual Finite Element Complex on the Barycentric Refinement," *Mathematics of Computation*, vol. 76, no. 260, pp. 1743–1769, 2007, publisher: American Mathematical Society. [Online]. Available: <https://www.jstor.org/stable/40234460>
- [17] R. Graglia, D. Wilton, and A. Peterson, "Higher order interpolatory vector bases for computational electromagnetics," *IEEE Transactions on Antennas and Propagation*, vol. 45, no. 3, pp. 329–342, Mar. 1997, conference Name: IEEE Transactions on Antennas and Propagation.
- [18] C. F. Bohren and D. R. Huffman, *Absorption and Scattering of Light by Small Particles*. Wiley, 1998.
- [19] L.-W. Li, X.-K. Kang, and M.-S. Leong, *Spheroidal Wave Functions in Electromagnetic Theory*. John Wiley & Sons, Apr. 2004.
- [20] R. Garbacz, "Modal expansions for resonance scattering phenomena," *Proceedings of the IEEE*, vol. 53, no. 8, pp. 856–864, 1965, publisher: IEEE.
- [21] Y. Chang and R. Harrington, "A surface formulation for characteristic modes of material bodies," *IEEE Transactions on Antennas and Propagation*, vol. 25, no. 6, pp. 789–795, Nov. 1977, conference Name: IEEE Transactions on Antennas and Propagation.
- [22] R. Harrington, J. Mautz, and Yu Chang, "Characteristic modes for dielectric and magnetic bodies," *IEEE Transactions on Antennas and Propagation*, vol. 20, no. 2, pp. 194–198, Mar. 1972.
- [23] Y. Chen and C.-F. Wang, *Characteristic Modes: Theory and Applications in Antenna Engineering*. John Wiley & Sons, June 2015, google-Books-ID: suobBgAAQBAJ.
- [24] M. Faenzi, G. Minatti, D. González-Ovejero, F. Caminita, E. Martini, C. Della Giovampola, and S. Maci, "Metasurface Antennas: New Models, Applications and Realizations," *Scientific Reports*, vol. 9, no. 1, p. 10178, July 2019, number: 1 Publisher: Nature Publishing Group. [Online]. Available: <https://www.nature.com/articles/s41598-019-46522-z>
- [25] R. F. Harrington, *Field computation by moment methods*. Wiley-IEEE Press, 1993.
- [26] C. Forestiere, G. Gravina, G. Miano, M. Pascale, and R. Tricarico, "Electromagnetic modes and resonances of two-dimensional bodies," *Physical Review B*, vol. 99, no. 15, p. 155423, Apr. 2019, publisher: American Physical Society. [Online]. Available: <https://link.aps.org/doi/10.1103/PhysRevB.99.155423>
- [27] I. D. Mayergoyz, D. R. Fredkin, and Z. Zhang, "Electrostatic (plasmon) resonances in nanoparticles," *Phys. Rev. B*, vol. 72, no. 15, p. 155412, Oct. 2005, publisher: American Physical Society. [Online]. Available: <https://link.aps.org/doi/10.1103/PhysRevB.72.155412>
- [28] G. Miano, G. Rubinacci, and A. Tamburrino, "Numerical Modeling for the Analysis of Plasmon Oscillations in Metallic Nanoparticles," *IEEE Transactions on Antennas and Propagation*, vol. 58, no. 9, pp. 2920–2933, Sept. 2010, conference Name: IEEE Transactions on Antennas and Propagation.
- [29] C. Forestiere, G. Miano, G. Rubinacci, M. Pascale, A. Tamburrino, R. Tricarico, and S. Ventre, "Magnetoquasistatic resonances of small dielectric objects," *Phys. Rev. Research*, vol. 2, no. 1, p. 013158, Feb. 2020, publisher: American Physical Society. [Online]. Available: <https://link.aps.org/doi/10.1103/PhysRevResearch.2.013158>
- [30] C. Forestiere, G. Miano, M. Pascale, and R. Tricarico, "Quantum theory of radiative decay rate and frequency shift of surface plasmon modes," *Physical Review A*, vol. 102, no. 4, p. 043704, Oct. 2020, publisher: American Physical Society. [Online]. Available: <https://link.aps.org/doi/10.1103/PhysRevA.102.043704>
- [31] C. Forestiere, G. Miano, and G. Rubinacci, "Resonance frequency and radiative Q-factor of plasmonic and dielectric modes of small objects," *Phys. Rev. Research*, vol. 2, no. 4, p. 043176, Nov. 2020, publisher: American Physical Society. [Online]. Available: <https://link.aps.org/doi/10.1103/PhysRevResearch.2.043176>
- [32] C. Forestiere and G. Miano, "Time-domain formulation of electromagnetic scattering based on a polarization-mode expansion and the principle of least action," *Physical Review A*, vol. 104, no. 1, p. 013512, July 2021, publisher: American Physical Society. [Online]. Available: <https://link.aps.org/doi/10.1103/PhysRevA.104.013512>
- [33] G. Vecchi, L. Matekovits, P. Pirinoli, and M. Orefice, "Hybrid spectral-spatial method for the analysis of printed antennas," *Radio Science*, vol. 31, no. 5, pp. 1263–1270, Sept. 1996, conference Name: Radio Science.
- [34] —, "A numerical regularization of the EFIE for three-dimensional planar structures in layered media (invited article)," *International Journal of Microwave and Millimeter-Wave Computer-Aided Engineering*, vol. 7, no. 6, pp. 410–431, 1997, _eprint: <https://onlinelibrary.wiley.com/doi/pdf/10.1002/%28SICI%291522-6301%28199711%297%3A6%3C410%3A%3AAID-MMCE4%3E3.0.CO%3B2-R>. [Online]. Available: <https://onlinelibrary.wiley.com/doi/abs/10.1002/%28SICI%291522-6301%28199711%297%3A6%3C410%3A%3AAID-MMCE4%3E3.0.CO%3B2-R>
- [35] A. Nosich, "The method of analytical regularization in wave-scattering and eigenvalue problems: foundations and review of solutions," *IEEE Antennas and Propagation Magazine*, vol. 41, no. 3, pp. 34–49, June 1999, conference Name: IEEE Antennas and Propagation Magazine.
- [36] M. Burton and S. Kashyap, "A study of a recent, moment-method algorithm that is accurate to very low frequencies," *Applied Computational Electromagnetics Society Journal*, vol. 10, pp. 58–68, 1995, publisher: APPLIED COMPUTATIONAL ELECTROMAGNETICS SOCIETY INC.
- [37] H. Golub and C. F. V. Loan, *Matrix Computations*. Baltimore, MD: Johns Hopkins University Press, 1983.
- [38] R. Graglia, "On the numerical integration of the linear shape functions times the 3-D Green's function or its gradient on a plane triangle," *IEEE Transactions on Antennas and Propagation*, vol. 41, no. 10, pp. 1448–1455, Oct. 1993, conference Name: IEEE Transactions on Antennas and Propagation.
- [39] D. R. Wilton and A. W. Glisson, "On improving the electric field integral equation at low frequencies," Los Angeles, CA, June 1981, pp. 22–24.
- [40] G. Vecchi, "Loop-star decomposition of basis functions in the discretization of the EFIE," *IEEE Transactions on Antennas and Propagation*, vol. 47, no. 2, pp. 339–346, Feb. 1999, conference Name: IEEE Transactions on Antennas and Propagation.
- [41] F. P. Andriulli, "Loop-Star and Loop-Tree Decompositions: Analysis and Efficient Algorithms," *IEEE Transactions on Antennas and Propagation*, vol. 60, no. 5, pp. 2347–2356, May 2012, conference Name: IEEE Transactions on Antennas and Propagation.

- [42] G. Miano and F. Villone, "A surface integral formulation of Maxwell equations for topologically complex conducting domains," *IEEE Transactions on Antennas and Propagation*, vol. 53, no. 12, pp. 4001–4014, Dec. 2005, conference Name: IEEE Transactions on Antennas and Propagation.
- [43] J.-S. Zhao and W. C. Chew, "Integral equation solution of Maxwell's equations from zero frequency to microwave frequencies," *IEEE Transactions on Antennas and Propagation*, vol. 48, no. 10, pp. 1635–1645, Oct. 2000, conference Name: IEEE Transactions on Antennas and Propagation.
- [44] S. Chen, W. C. Chew, J. Song, and J.-S. Zhao, "Analysis of low frequency scattering from penetrable scatterers," *IEEE Transactions on Geoscience and Remote Sensing*, vol. 39, no. 4, pp. 726–735, Apr. 2001, conference Name: IEEE Transactions on Geoscience and Remote Sensing.
- [45] P. Ylä-Oijala, H. Wallén, D. C. Tzarouchis, and A. Sihvola, "Surface Integral Equation-Based Characteristic Mode Formulation for Penetrable Bodies," *IEEE Transactions on Antennas and Propagation*, vol. 66, no. 7, pp. 3532–3539, July 2018, conference Name: IEEE Transactions on Antennas and Propagation.
- [46] M. Taskinen and P. Ylä-Oijala, "Current and charge Integral equation formulation," *IEEE Transactions on Antennas and Propagation*, vol. 54, no. 1, pp. 58–67, Jan. 2006, conference Name: IEEE Transactions on Antennas and Propagation.
- [47] Z. G. Qian and W. C. Chew, "An augmented electric field integral equation for high-speed interconnect analysis," *Microwave and Optical Technology Letters*, vol. 50, no. 10, pp. 2658–2662, 2008, eprint: <https://onlinelibrary.wiley.com/doi/pdf/10.1002/mop.23736>. [Online]. Available: <https://onlinelibrary.wiley.com/doi/abs/10.1002/mop.23736>
- [48] G. Mie, "Beiträge zur Optik trüber Medien, speziell kolloidaler Metallösungen," *Annalen der physik*, vol. 330, no. 3, pp. 377–445, 1908, publisher: Wiley Online Library.
- [49] P. B. Johnson and R. W. Christy, "Optical Constants of the Noble Metals," *Phys. Rev. B*, vol. 6, no. 12, pp. 4370–4379, Dec. 1972, publisher: American Physical Society. [Online]. Available: <https://link.aps.org/doi/10.1103/PhysRevB.6.4370>
- [50] J. A. Schuller, E. S. Barnard, W. Cai, Y. C. Jun, J. S. White, and M. L. Brongersma, "Plasmonics for extreme light concentration and manipulation," *Nat. Mater.*, vol. 9, pp. 193–204, 2010.
- [51] P.-O. Persson and G. Strang, "A Simple Mesh Generator in Matlab," *SIAM Review*, vol. 46, no. 2, pp. 329–345, 2004, publisher: Society for Industrial and Applied Mathematics. [Online]. Available: <https://www.jstor.org/stable/20453511>